Hindawi
Shock and Vibration
Volume 2018, Article ID 2431980, 14 pages
https://doi.org/10.1155/2018/2431980

Research Article

Reduction of Vehicle-Induced Vibration of Railway Bridges due to Distribution of Axle Loads through Track

Zhibin Jin,[1] **Bo Huang**,[1] **Juanjuan Ren**,[1] **and Shiling Pei**[2]

[1]*Department of Bridge Eng., Southwest Jiaotong University, Chengdu, China*
[2]*Department of Civil and Environmental Eng., Colorado School of Mines, Golden, USA*

Correspondence should be addressed to Zhibin Jin; jinzhibin1979@163.com and Juanjuan Ren; renjuanjuan1983@hotmail.com

Received 26 April 2018; Revised 1 August 2018; Accepted 8 August 2018; Published 12 September 2018

Academic Editor: Pedro Galvín

Short span railway bridges are prone to resonate caused by dynamic train axle loads, which were usually modeled as moving point loads on the bridge in many numerical studies. In reality, the axle weight of the train is a spread load for the bridge deck because of the transfer of the track structure. Previous numerical studies indicated that the spread axle load distributed through the track structure significantly reduces bridge responses compared to the point load model. In this study, the reduction effect is investigated analytically by solving the moving load problem for both the point load and the spread load cases. The analytical solution reveals that bridge responses from the spread load model can be obtained by filtering bridge responses from the point load model. The filter function is exactly the Fourier transform (FT) of the load spreading function. Based on this relationship, a reduction coefficient reflecting the load spreading effect on bridge responses is derived. Through numerical examples, the accuracy of this proposed reduction coefficient is validated not only for the moving load models but also for vehicle-bridge interaction (VBI) problems.

1. Introduction

The dynamic interaction between vehicle and bridge has attracted great attention in recent decades with the rapid expansion of high-speed railway construction worldwide. Currently, detailed vehicle-bridge interaction (VBI) models [1–4] considering the vibration of both the vehicle and the bridge have been developed to evaluate the bridge performance due to passing trains. A more detailed model including the track structure in the VBI system has been proposed by Zhai et al. [5].

Although the VBI time-history simulation is very robust, it is very computationally expensive to be used by practicing engineers, especially in the preliminary design stage. Fortunately, closed-form solutions to some moving load (ML) problems are available; and these can provide reasonable estimation for bridge vibrations. Most of these closed-form solutions are pertaining to the vibration of the simply supported beam under moving loads. For example, Timoshenko [6] solved the moving load problem analytically for a single-point load. Fryba [7] derived the solution for a continuously distributed load. Yang et al. [8], Savin [9], Domínguez [10], and Xia et al. [11], among others, developed solutions for a group of successive point loads. On the basis of these closed-form solutions, design code style formulas have been proposed in [8–10] to estimate the peak bridge response under passing vehicles. Among these formulas, the decomposition of excitation in resonance (DER) proposed in [10] was adopted by the Eurocode [12].

Needless to say, the ML model excludes the VBI effect. To make up this deficiency of the ML model, many efforts have been made to quantify the VBI effect on the bridge responses. For example, the UIC document [13] approximately accounts for the VBI effect on bridge vibration by adding some damping to the bridge structure. Doménech et al. [14] checked the accuracy of the increased damping approach in [13] and investigated the key parameters controlling the VBI effect. Museros et al. [15] provided a quantitative insight into the VBI effect on bridge vibration via numerical simulations.

Besides the VBI effect, ML models do not account for the effect of the track structure on bridge responses. These effects include the following [16]: (1) the vibration of the track structure, (2) additional constraints applied on the bridge ends by the track, and (3) axle load distributed through track

on the bridge deck. Several authors [17–19] concluded that the vibration of the track (the first effect) has a minor effect on bridge vibration. Rebelo et al. [20] suggested that the constraints provided by the continuous track on bridge ends (the second effect) can be represented by longitudinal springs added at bridge ends.

The third effect of the track structure, redistribution of the point axle loads, has been shown to reduce the bridge responses considerably, especially for short span cases. Museros et al. [15] modeled the moving loads on the bridge as a sequence of block-distributed loads and found that the point load model may unrealistically overpredict the bridge vibration for short span bridges. They proposed two formulas to account for the reduction effect of load spreading on bridge response. Rehnström and Daniel [21] investigated the influence of various shapes of load distribution on bridge vibrations and found that the triangular load shape gives the most similar result to that of the model including rail and ballast. The UIC document [22] also provided a graph of the reduction coefficient through numerical simulations with the specific load distribution width of 2.5 m and 3 m.

All these existing studies on the load spreading effect were carried out numerically in the time domain for specific load shapes. In this study, the load spreading effect will be investigated analytically in the frequency domain. This frequency domain method helps to reveal the mechanism of the vibration reduction provided by spreading of the axle load and leads to more concise formulas that are applicable to various load distribution shapes.

2. Distribution of Axle Load by the Track Structure

The track structure, consisting of rails, sleepers, and ballast, spreads each axle load over a finite area on the deck. The shape of load spreading on the bridge deck depends on various factors, including the location of the axle, the thickness, and the elastic modulus of the ballast, as concluded in [23]. The load spreading shape approaches a triangle when an axle locates on a single sleeper, and it changes to a trapezoid when the axle moves to the middle of two adjacent sleepers. However, it was found that the shifting of load shape from triangle to trapezoid has a very small effect on the bridge vibration [21]. Therefore, only the triangular distribution will be considered in this study.

A unit axle load of triangular distribution (Figure 1(a)) can be written as

$$s_{\Delta}(x) = \begin{cases} \dfrac{1-(x/w)}{w}, & \dfrac{x}{w} \in [0,1], \\ \dfrac{1+(x/w)}{w}, & \dfrac{x}{w} \in [-1,0], \\ 0, & else, \end{cases} \tag{1}$$

where $2w$ is the load spreading width over the bridge deck, and the value of 3 m is suggested in [21] for typical ballasted tracks.

Eurocode (EC) [24] proposed the axle load distribution pattern in Figure 1(b), where the axle load is carried by three adjacent sleepers and each spreads its received load through the ballast as a block load. In Figure 1(b), "a" is the space between two adjacent sleepers and "b" is the width of each of the three-block loads. Although the solution procedure in this paper is applicable to any load shape (such as the load distribution on Winkler foundation), only the triangular shape (Figure 1(a)) and Eurocode load shape (Figure 1(b)) which are of practical significance will be discussed hereafter.

3. Bridge Vibration due to Moving Point Loads and Spread Loads

3.1. Equations of Motion of the Bridge due to Moving Loads. The vertical displacement $y(x,t)$ of a Bernoulli–Euler beam loaded by N spread loads moving at the speed v can be described by the equation:

$$m(x)\frac{\partial^2 y}{\partial t^2} + \frac{\partial^2}{x^2}\left[\mathrm{EI}(x)\frac{\partial^2 y}{\partial x^2}\right] + \chi\frac{\partial y}{\partial t} = \sum_{k=1}^{N} F_k s(x - vt + l_k) \cdot \Pi(x), \tag{2}$$

where $m(x)$, $\mathrm{EI}(x)$, and χ are the mass per length, bending stiffness, and damping coefficient of the bridge, respectively, F_k is the load from the $k-$th axle of the train, $s(x)$ is the function of the load shape, and l_k is the distance between the $k-$th and the first axle, as shown in Figure 2. The function $\Pi(x) = [1|x \in (0,\ L);\ 0|\mathrm{else}]$ indicates whether the load is on the bridge or not, where L is the bridge span.

According to the modal superposition method, the bridge displacement $y(x,t)$ in (2) can be expressed as

$$y(x,t) = \sum_{i=1}^{+\infty} q_i(t)\phi_i(x), \tag{3}$$

where $\phi_i(x)$ is the $i-$th mode of the bridge which is assumed to be normalized with respect to the mass of the bridge and $q_i(t)$ is the $i-$th modal displacement.

By substituting (3) into (2), multiplying $\phi_i(x)$ to both sides, and then integrating with respect to x from 0 to L, the dynamic equation of the bridge is decomposed into n single-degree-of-freedom (SDOF) dynamic systems as

$$\ddot{q}_i + 2\zeta_i\omega_{\mathrm{b},i}\dot{q}_i + \omega_{\mathrm{b},i}^2 q_i = p_i(vt) \text{ with } i = 1,\ 2,\ \ldots,\ n. \tag{4}$$

The right-hand side (RHS) of (4) is the $i-$th modal force written as

$$p_i(vt) = \sum_{k=1}^{N}\int_{-\infty}^{\infty} F_k s(x - vt + l_k)\phi(x)\Pi(x)\ dx. \tag{5}$$

By defining $\iota = vt$ as the distance traveled by the train at the time instant "t," then (4) can be written as

$$v^2\frac{d^2 q_i(\iota)}{d\iota^2} + 2\zeta_i\omega_{\mathrm{b},i}v\frac{dq_i(\iota)}{d\iota} + \omega_{\mathrm{b},i}^2 q_i = p_i(\iota). \tag{6}$$

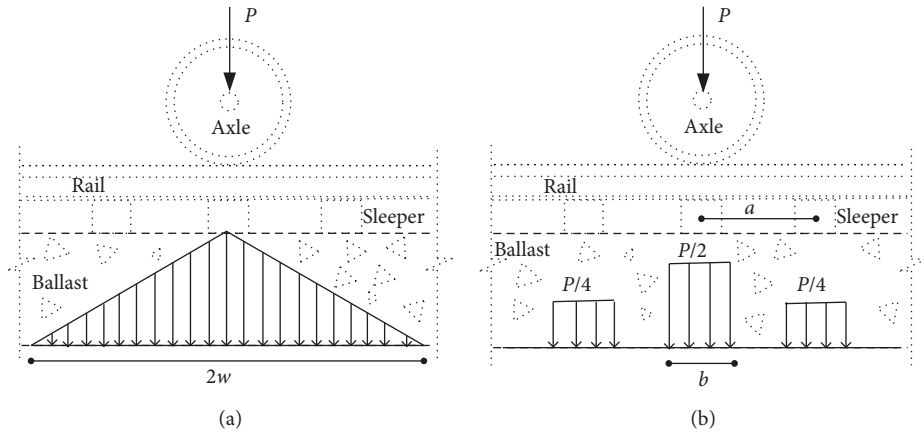

Figure 1: Shapes of load distribution on the bridge deck. (a) Triangular distribution. (b) Three-block distribution in Eurocode.

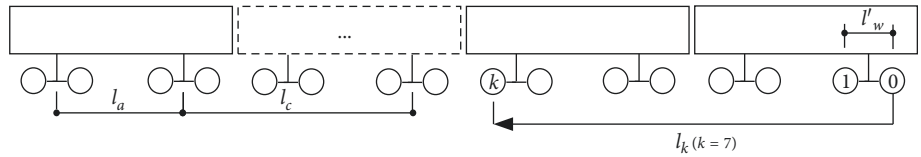

Figure 2: Spacing of axles in a train.

3.2. Modal Force on Bridge from Moving Loads. By replacing vt with ι in (5), the modal force at the RHS of (6) can be written as

$$p(\iota) = \sum_{k=1}^{N} \int_{-\infty}^{\infty} F_k s(x - \iota + l_k)\phi(x)\Pi(x)\,dx. \tag{7}$$

For the sake of conciseness, the subscript "i" in (4) denoting the mode sequence will be omitted hereafter.

Equation (7) is the sum of N integrations each corresponds to the contribution of one axle. By replacing x with $x - l_k$ for the $k-$th integration in (7), i.e., moving the origin of the $k-$th integrand rightward for l_k, (7) can be written as

$$p(\iota) = \int_{-\infty}^{\infty} \left[s(x - \iota) \sum_{k=1}^{N} F_k \phi(x - l_k)\Pi(x - l_k) \right] dx. \tag{8}$$

Since all integrations in (7) have infinite limits, the sum of N integrands with different origins of "x" can be written in the compact form of (8).

The load shape for a point load is the Dirac function $\delta(x)$. Thus, the model force corresponding to point loads $p_{\downarrow}(\iota)$ can be obtained by replacing $s(\cdot)$ with $\delta(\cdot)$ in (8):

$$\begin{aligned} p_{\downarrow}(\iota) &= \sum_{k=1}^{N} \int_{-\infty}^{\infty} F_k \delta(x - \iota)\phi(x - l_k)\Pi(x - l_k)\,dx \\ &= \sum_{k=1}^{N} F_k \phi(\iota - l_k)\Pi(\iota - l_k), \end{aligned} \tag{9}$$

$$\text{or} \quad p_{\downarrow}(x) = \sum_{k=1}^{N} F_k \phi(x - l_k)\Pi(x - l_k). \tag{9a}$$

By comparing the RHSs of Equations (8) and (9a), it can be concluded that the modal force of spread loads and that of point loads is related by

$$p(\iota) = \int_{-\infty}^{\infty} s(x - \iota) p_{\downarrow}(x)\,dx. \tag{10}$$

The RHS of (10) represents the weighted averaging of $p_{\downarrow}(x)$ with the weight function $s(x - \iota)$. Therefore, (10) reveals that averaging the model force of point loads, using the load shape function as the weight function, leads to the model force of spread loads.

Since the load spread shape is symmetrical, the load spread function $s(x)$ is even, i.e., $s(x - \iota) = s(\iota - x)$. Thus, (10) can be rewritten as the following convolution form:

$$p(\iota) = \int_{-\infty}^{\infty} s(\iota - x) p_{\downarrow}(x)\,dx. \tag{10a}$$

From the theory of Fourier transform (FT), the convolution of (10a) in the time or space domain is easier to be calculated in the frequency domain. The frequency domain counterparts of $p(x)$, $p_{\downarrow}(x)$, and $s(x)$ are the following Fourier transform as

$$P(\Omega) = \int_{-\infty}^{\infty} p(x)\exp(j\Omega x)\,dx, \tag{11a}$$

$$P_{\downarrow}(\Omega) = \int_{-\infty}^{\infty} p_{\downarrow}(x)\exp(j\Omega x)\,dx, \tag{11b}$$

$$S(\Omega) = \int_{-\infty}^{\infty} (x)\exp(j\Omega x)\,dx, \tag{11c}$$

where j is the imaginary unit and Ω is space frequency with the unit of rad/m and is related to the wavelength λ by

$$\Omega = \frac{2\pi}{\lambda}. \tag{12}$$

The theory of Fourier transform has proven that the convolution in the space domain is equivalent to the multiplication in the frequency domain. Therefore, from the convolution of (10a), it can be concluded that

$$P(\Omega) = S(\Omega)P_{\downarrow}(\Omega). \tag{13}$$

Equation (13) reveals that filtering the model force of the point loads gives the model force of the spread loads. And the filter function $S(\Omega)$ is just the Fourier transform of the load shape function $s(x)$.

3.3. Frequency Domain Solution to Bridge Vibration. The steady-state response of the bridge from moving spread load governed by (6) can be solved in the frequency domain. By taking the FT for both sides of (6), one gets

$$\left(-v^2\Omega^2 + 2j\zeta\omega_b v\Omega + \omega_b^2\right)Q(\Omega) = P(\Omega), \tag{14}$$

where $Q(\Omega)$ is the FT of $q(\iota)$. By defining $\Omega_b = \omega_b/v$, where ω_b is the natural frequency of the bridge, $Q(\Omega)$ can be solved from (14) as

$$Q(\Omega) = \frac{1}{(v\Omega_b)^2}\frac{P(\Omega)}{1-(\Omega/\Omega_b)^2 + 2j\zeta(\Omega/\Omega_b)}. \tag{15}$$

Similarly, the FT of bridge vibration due to moving point loads reads

$$Q_{\downarrow}(\Omega) = \frac{1}{(v\Omega_b)^2}\frac{P_{\downarrow}(\Omega)}{1-(\Omega/\Omega_b)^2 + 2j\zeta(\Omega/\Omega_b)}. \tag{16}$$

By comparing equations (15), (16), and (13), the bridge vibration due to moving spread loads and point loads can be related by

$$Q(\Omega) = S(\Omega)Q_{\downarrow}(\Omega). \tag{17}$$

Equation (17) reveals that the bridge response due to spread loads can be easily obtained by filtering that due to point loads. This filtering process in the frequency domain is equivalent to the following weighted averaging in the time domain.

$$q(\iota) = \int_{-\infty}^{\infty} s(l-x)q_{\downarrow}(x)\,dx. \tag{18}$$

Equations (17) and (18) are not dependent on neither the mode nor the natural frequency of the bridge. Thus, these equations are applicable for all configurations of bridge. From equations (17) and (18), once the time history of bridge response due to point loads is known, by filtering or weighted averaging, the bridge response due to spread loads can be obtained easily.

In the above derivation, the only approximation lies in the omission of the transient response. But this approximation is acceptable, since, for short to medium span bridges traversed by long trains, the bridge vibration is dominated by the steady-state response.

3.4. Track Transfer Function for Spread Loads. The filter function for load shapes $s(x)$ in Figure 1 can be obtained by (11c) as

$$S_{\Delta}(\Omega) = \frac{1}{(w\Omega/2)^2}\sin^2\left(\frac{w\Omega}{2}\right) \quad \text{(triangular load)}, \tag{19}$$

$$S_{EC}(\Omega) = \frac{\sin(b\Omega/2)}{b\Omega/2}\cdot\cos^2\left(\frac{a\Omega}{2}\right) \quad \text{(EC block load)}, \tag{20}$$

where the dimensions "w," "a," and "b" are shown in Figure 1.

The filter functions (19) and (20) are plotted in Figure 3 with $2w = 3$ m, $a = 0.65$ m, and $b = 0.605$ m. It can be seen that the track acts as a low-pass filter. This filtering effect of track structure on bridge vibration has been observed through numerical and experimental investigations in [19]. Here, the specific filtering functions are obtained.

3.5. Reduction Coefficient of Bridge Vibration due to Load Distribution through Track. According to (17) and (18), it is possible to approximate the bridge vibration due to spread loads by modifying the one from the point loads. And this approach is preferable in engineering practice, since the problem of moving point load is easy to be programmed. For simply supported bridges, closed-form solution has been obtained for the moving point load model, based on which Eurocode adopted the so-called DER formula to estimate the maximum bridge responses.

From the frequency domain solution in (15) and (16), the resonant component of the bridge vibration corresponds to the space frequency $\Omega = \Omega_b$, or the time frequency $\omega \triangleq v\Omega = v\Omega_b \triangleq \omega_b$, where ω_b is the natural frequency of the bridge. Previous studies [16] have shown that the bridge vibration is dominated by the resonant component. Therefore, by only including the resonant component in (17) and (18), the amplitude of bridge vibration approximates

$$\begin{aligned} |q(\iota)|_{\max} &\approx \frac{1}{(v\Omega_b)^2}\left|\frac{P(\Omega)S(\Omega)}{1-(\Omega/\Omega_b)^2 + 2j\zeta(\Omega/\Omega_b)}\right|_{\Omega=\Omega_b} \\ &= \frac{1}{(v\Omega_b)^2}\left|\frac{P(\Omega_b)S(\Omega_b)}{2\zeta}\right| \quad \text{(spread load)}, \end{aligned} \tag{21}$$

$$\begin{aligned} \left|q_{\downarrow}(\iota)\right|_{\max} &\approx \frac{1}{(v\Omega_b)^2}\left|\frac{P_{\downarrow}(\Omega)}{1-(\Omega/\Omega_b)^2 + 2j\zeta(\Omega/\Omega_b)}\right|_{\Omega=\Omega_b} \\ &= \frac{1}{(v\Omega_b)^2}\left|\frac{P(\Omega_b)}{2\zeta}\right| \quad \text{(point load)}. \end{aligned} \tag{22}$$

The reduction coefficient from load spreading is defined as

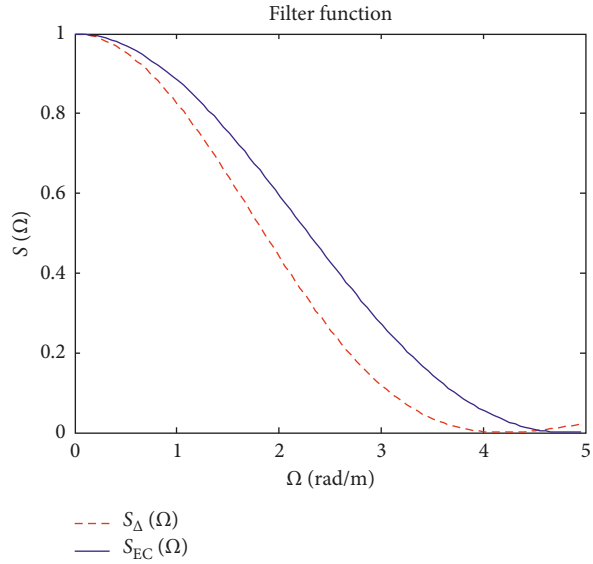

Figure 3: Low-pass filter for load spreading effect.

$$R = \frac{|q(t)|_{\max}}{\left|q_{\downarrow}(t)\right|_{\max}}. \tag{23}$$

By substituting (21), (22), and $\Omega_b = \omega_b/v$ into (23), one gets

$$R \approx \left|S\left(\frac{\omega_b}{v}\right)\right| = \left|S\left(\frac{2\pi}{\lambda_b}\right)\right|, \tag{24}$$

where $\lambda_b = 2\pi v/\omega_b$ is the wavelength of excitation defined in [12] as the ratio of the vehicle speed to the bridge natural frequency. Equation (24) shows that this reduction coefficient depends solely on the wavelength of excitation, which has been noticed by Museros et al. [15].

Equation (24) provides a closed-form reduction coefficient R for the load spreading effect on bridge vibration. Once the maximum bridge response from the point load is known, the maximum bridge response from the spread load model can be estimated by

$$|q(\iota)|_{\max} = R\left|q_{\downarrow}(\iota)\right|_{\max} = \left|S\left(\frac{2\pi}{\lambda_b}\right)\right|\left|q_{\downarrow}(\iota)\right|_{\max}. \tag{25}$$

It can be proved that the reduction coefficients for bridge displacement, velocity, and acceleration are the same.

The UIC document [22] also proposed a graphical reduction coefficient for load spreading effect through numerical simulations. This graph gives two reduction curves for the specific spread width of 2.5 m and 3 m. Unlike the UIC curves, (24) is applicable to various load distribution shapes with arbitrary width. Moreover, (24) reveals the physical mechanism of vibration reduction due to load spreading.

4. Reduction of Vehicle-Bridge Coupling Vibration due to Load Spreading

In conventional VBI models, the action of vehicles on the bridge is assumed to be point loads (Figure 4(a)), i.e., the load distribution provided by the track structure is disregarded. The vehicle-track-bridge interaction model [5] can consider this load distribution effect, but increases the degrees of freedom of the system dramatically. In this section, a VBI model with spread loads (Figure 4(b)) is proposed to reflect the main contribution of the track structure.

For simplicity, we only consider one moving oscillator moving on the bridge. This moving oscillator has been used successfully in assessing the effect of vehicle-bridge dynamic interaction in [25]. The equation of motion of the oscillator reads

$$M_2 \cdot \ddot{Z}(t) + c_1 \cdot \left[\dot{Z}(t) - \left.\frac{\partial y(x,t)}{\partial t}\right|_{x=vt}\right] + k_1 \cdot \left[Z(t) - y(x,t)|_{x=vt}\right] = 0. \tag{26}$$

For the spread load model (Figure 4(b)), the motion equation of the bridge reads

$$m \cdot \frac{\partial^2 y(x,t)}{\partial t^2} + \chi \cdot \frac{\partial y(x,t)}{\partial t} + \mathrm{EI} \cdot \frac{\partial^4 y(x,t)}{\partial x^4} = s(x-vt) \cdot \left\{(M_1 + M_2) \cdot g - M_1 \cdot \frac{\partial^2 y(vt,t)}{\partial t^2} + k_1 \cdot [Z(t) - y(vt,t)] + c_1 \cdot \left[\dot{Z}(t) - \frac{\partial y(vt,t)}{\partial t}\right]\right\}, \tag{27}$$

where M_1 and M_2 are mass of the wheel and the truck, respectively, $Z(t)$ is the vertical displacement of the oscillator, c_1 and k_1 denote the damping and stiffness of the oscillator, respectively.

By substituting the mode shape of (3) into (26), one obtains

$$M_2 \cdot \ddot{Z}(t) + c_1 \cdot [\dot{Z}(t) - \phi(vt)\dot{q}(t)] + k_1 \cdot [Z(t) - \phi(vt)q(t)] = 0. \tag{28}$$

By substituting the mode shape of (3) into (27) and then integrating both sides from 0 to L with respect to x, the bridge equation in terms of its modal displacement $q(t)$ reads

$$\ddot{q}(t) + 2\zeta\omega_b\dot{q}(t) + \omega_b^2 q(t) = \left\{(M_1 + M_2) \cdot g - M_1 \cdot \phi(vt)\ddot{q}(t) + k_1 \cdot [Z(t) - \phi(vt)q(t)] + c_1 \cdot [\dot{Z}(t) - \phi(vt)\dot{q}(t)]\right\} \times \int_0^L s(x-vt)\phi(x)\,dx. \tag{29}$$

Equations (28) and (29) are solved here using the subsystem iteration proposed in [26]. The process of the subsystem iteration is illustrated in Figure 5, where the superscript in the bracket denotes the iteration sequence. The iteration starts by assuming the oscillator to be stationary, that is, $Z^{(0)}(t) = \dot{Z}^{(0)}(t) = 0$. Then $Z^{(0)}(t)$ and $\dot{Z}^{(0)}(t)$ are substituted into (29) from which the bridge

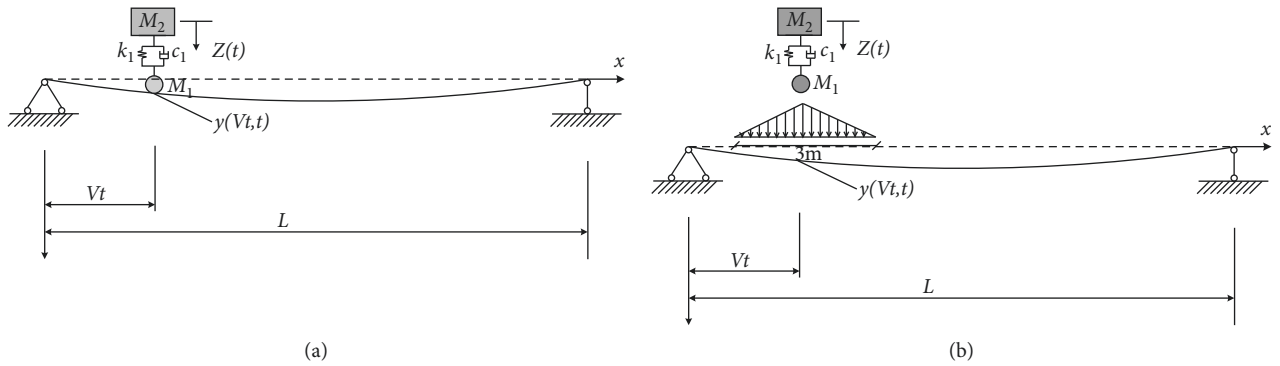

Figure 4: Moving oscillator models. (a) Point load. (b) Spread load.

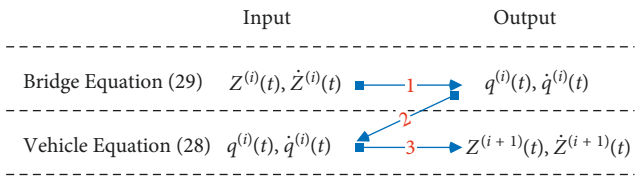

Figure 5: Information flow of the subsystem iteration.

vibration $q^{(0)}(t)$ and $\dot{q}^{(0)}(t)$ are solved. In the following step, $q^{(0)}(t)$ and $\dot{q}^{(0)}(t)$ are substituted into (28), and the oscillation responses $Z^{(1)}(t)$ and $\dot{Z}^{(1)}(t)$ are obtained. This process continues until the bridge and oscillator response converges.

This iteration process can be written as the following form.

$$\begin{aligned}
&\left[1 + M_1 \cdot \phi(vt)\right]\ddot{q}^{(i)} + \left[2\zeta\omega_b + c_1\phi(vt)\right]\dot{q}^{(i)} + \left[\omega_b^2 + k\phi(vt)\right]q^{(i)} \\
&\quad = \left[(M_1 + M_2)g + k_1 Z^{(i)}(t) + c_1\dot{Z}^{(i)}(t)\right]\int_0^L s(x - vt)\phi(x)\,dx, \\
&M_2 \cdot \ddot{Z}^{(i+1)}(t) + c_1 \cdot \dot{Z}^{(i+1)}(t) + k_1 \cdot Z^{(i+1)}(t) \\
&\quad = \left[k_1 q^{(i)}(t) + c_1\dot{q}^{(i)}(t)\right]\phi(vt), \quad i = 0,\ 1,\ 2,\ \ldots.
\end{aligned} \tag{30}$$

The superscripts "i" and "$i + 1$" denote the i – th and the $(i + 1)$ – th iteration. All initial conditions of the bridge and the oscillator are assigned to zero, i.e., $Z^{(i)}(0) = 0$, $\dot{Z}^{(i)}(0) = 0$, $q^{((i)}(0) = 0$, and $\dot{q}^{(i)}(0) = 0$.

The solution of substructure iteration algorithm can be rewritten as the following Duhamel's integration:

$$q^{(0)}(t) = \int_0^t h_q(t,\tau)(M_1 + M_2)g\,d\tau, \tag{31}$$

$$Z^{(i+1)}(t) = \int_0^t h_Z(t,\tau)\phi(v\tau)\left[k_1 q^{(i)}(\tau) + c_1\dot{q}^{(i)}(\tau)\right]d\tau, \tag{32}$$

$$q^{(i+1)}(t) = \int_0^t h_q(t,\tau)\phi(v\tau)\left[k_1 Z^{(i)}(\tau) + c_1\dot{Z}^{(i)}(\tau)\right]d\tau, \quad i = 0, 1, 2, \ldots, \tag{33}$$

where $h_q(t,\tau)$ is the impulse function of the bridge and $h_Z(t,\tau)$ is that of the oscillator.

The final solution of the system is the following series:

$$\begin{aligned}
q(t) &= \sum_{i=0}^{\infty} q^{(i)}(t), \\
Z(t) &= \sum_{i=0}^{\infty} Z^{(i)}(t).
\end{aligned} \tag{34}$$

VBI models using the point load and the spread load pattern are different only in the bridge impulse function. The impulse function of the point load $h_{q,\downarrow}(t,\tau)$ and that of the spread load $h_q(t,\tau)$ can be related approximately through (25). Therefore,

$$h_q(t,\tau) \approx R h_{q,\downarrow}(t,\tau). \tag{35}$$

By substituting (35) into (32) and (33), the solutions of system response from the spread load model and the one from the point load model can be related by

$$q^{(i)}(t) \approx R^{i+1} q_{\downarrow}^{(i)}(t), \tag{36}$$

$$Z^{(i)}(t) \approx R^i Z_{\downarrow}^{(i)}(t), \quad i = 0, 1, 2, \ldots. \tag{37}$$

In equations (35)–(37), the subscript "$\downarrow$" denotes variables correspondent to the point load model. The bridge response reduction for the VBI model by load spreading reads

$$R' = \frac{q(t)}{q_{\downarrow}(t)} = \frac{\sum_{i=0}^{\infty} q^{(i)}(t)}{\sum_{i=0}^{\infty} q_{\downarrow}^{(i)}(t)}. \tag{38}$$

By substituting (36) and (37) into (38), the bridge response reduction for VBI model is

$$R' = \frac{\sum_{i=0}^{\infty} R^{i+1} q_{\downarrow}^{(i)}(t)}{\sum_{i=0}^{\infty} q_{\downarrow}^{(i)}(t)} = R\frac{q_{\downarrow}^{(0)}(t) + \sum_{i=1}^{\infty} R^i q_{\downarrow}^{(i)}(t)}{q_{\downarrow}^{(0)}(t) + \sum_{i=1}^{\infty} q_{\downarrow}^{(i)}(t)} \approx R. \tag{39}$$

The approximation in (39) holds since $q_{\downarrow}^{(i)}(t)$ $(i = 1, 2, 3, \ldots)$ are small terms compared with $q_{\downarrow}^{(0)}(t)$ and $0 < R < 1$.

Is should be pointed out that, although the proof of (39) only uses one oscillator, it can be generalized to the VBI system with multiple vehicles.

5. Numerical Examples

5.1. Response Reduction due to Spread Load for Moving Load Model. A simply supported bridge with parameters listed in Table 1 is adopted to demonstrate the effect of load spreading on bridge vibrations. The train is composed of 9 identical cars with dimensions (Figure 2): $l_w = 2.5$ m, $l_a = 18.0$ m, and $l_c = 26.0$ m. The axle load of 84.378 kN is assumed to spread into a triangle with $2w = 3$ m (Figure 1(a)) and the three-block pattern with $a = 0.65$ m and $b = 0.605$ m (Figure 1(b)), respectively.

After sweeping the train speed from 100 to 400 km/h, the bridge resonance speed was found to be 290 km/h. At this speed, the acceleration time histories at midspan of the bridge due to point loads and spread loads are shown in Figure 6. Bridge acceleration was obtained using the Newmark-β method. In the following numerical simulations, only the first mode is included except where specified otherwise. It can be seen from Figure 6 that the load spreading reduces the bridge vibration considerably. The result of averaging (according to (18)) of the bridge acceleration due to point loads is also shown in Figure 6. It can be seen that, after weighted averaging, the bridge acceleration due to point loads coincides with the one due to spread loads.

The Fourier amplitude spectrum of the bridge acceleration at the resonance speed (290 km/h) is shown in Figure 7. There is a single peak at the spatial frequency $\Omega = 1.44$ rad/m which corresponds to the natural frequency of the bridge: $1.44\ (\text{rad/m}) \times 290/3.6\ (\text{m/s})/(2\pi) = 18.5$ Hz. This is expected since at resonance speed, the bridge vibration is dominated by its natural frequency. In Figure 7, the product of $S(\Omega)Q_{\downarrow}(\Omega)$ in (7) is also shown. It can be observed that the Fourier spectrum of bridge acceleration due to point loads $Q_{\downarrow}(\Omega)$ scaled by $S(\Omega)$ approximates the Fourier spectrum of bridge acceleration due to spread loads $Q(\Omega)$.

Figure 8 shows bridge acceleration due to point load, its weighted averaging, and that due to spread load at a nonresonance speed of 266 km/h. From Figure 8, the averaging of vibration due to point loads coincides with that due to spread loads. Figure 8 indicates even at nonresonance speeds, weighted averaging of bridge vibration from point loads still approaches that from spread loads.

The Fourier spectrum of these accelerations is plotted in Figure 9. Peaks at frequencies other than the bridge natural frequency can be observed in this spectrum plot. Similar to the resonance case, the Fourier spectrum of bridge vibration from point loads scaled by $S(\Omega)$ approaches that from spread loads.

The maximum bridge accelerations at the speed range from 100 to 400 km/h are shown in Figure 10. The bridge acceleration from point loads and spread loads and that due to point loads scaled by $|S(2\pi/\lambda_b)|$ according to (25) are plotted. Figure 10 indicates that the bridge vibration due to spread loads can be approximated by modifying that due to point loads using the factor $|S(2\pi/\lambda_b)|$.

In the above illustration, only the first mode that contributes most to the bridge responses is included. The effect of spread load on the 2nd and the 3rd modes is illustrated in Figure 11. From the Fourier spectrum of the bridge acceleration of the 2nd and the 3rd modes, the point load model introduces high-frequency components which are filtered out by the load spreading effect.

Table 1: Parameters of the simply supported bridge.

Variable	Meaning	Unit	Value
L	Bridge span	m	10
m	Mass of bridge per length	kg/m	9100
n_0	Natural frequency of the bridge	Hz	18.5
ζ_0	Damping ratio of the bridge	%	1

Figure 12 shows the reduction coefficient of bridge acceleration obtained from numerical simulations and the simplified formula (25). The reduction coefficients for the 1st, the 2nd, and the 3rd modal components of the bridge acceleration are compared. It can be seen that the spread load filters out more than 80% of the contribution of the second and the third modes. From Figure 12, the load spreading filters more contents for higher modes, because the load spreading effect acts as a low-pass filter as indicated in Figure 3. And this justified the omission of higher modes when calculating bridge acceleration using the moving spread load model.

5.2. Response Reduction due to Load Spreading for Vehicle-Bridge Interaction. Load spreading through track can also reduce the vehicle-bridge dynamic responses as indicated in [19]. We deduced in Section 4 that the reduction effect for the VBI model should approximate that for the moving load model. The reduction effect of spread load for VBI system is examined in this section.

The VBI system is modeled as a series of moving oscillators with their parameters shown in Figure 13. The bridge parameters are taken from Table 1. The values of the vehicle parameters in this example are listed in Table 2. The train is composed of 9 vehicles, modeled as 36 moving oscillators.

The vehicle-bridge dynamic response is obtained from the subsystem iteration in Section 4. In each iteration, the bridge and vehicle responses are calculated using the Newmark-β method.

The maximum bridge accelerations from the VBI model using the point load model and the spread load model are plotted in Figure 14. The bridge acceleration from the point load model scaled by $|S(2\pi/\lambda_b)|$ according to Equation (25) is also shown. It can be concluded that, for the VBI model, the bridge response from spread loads can be approximated by modifying that from point loads using (25).

6. Validation of the Reduction Coefficient for Load Spreading Effect

The vibration of eight bridges different in span, frequency, and mass are calculated numerically to demonstrate the accuracy of the reduction coefficient (25). The parameters of the eight bridges are listed in Table 3. The vehicle parameters

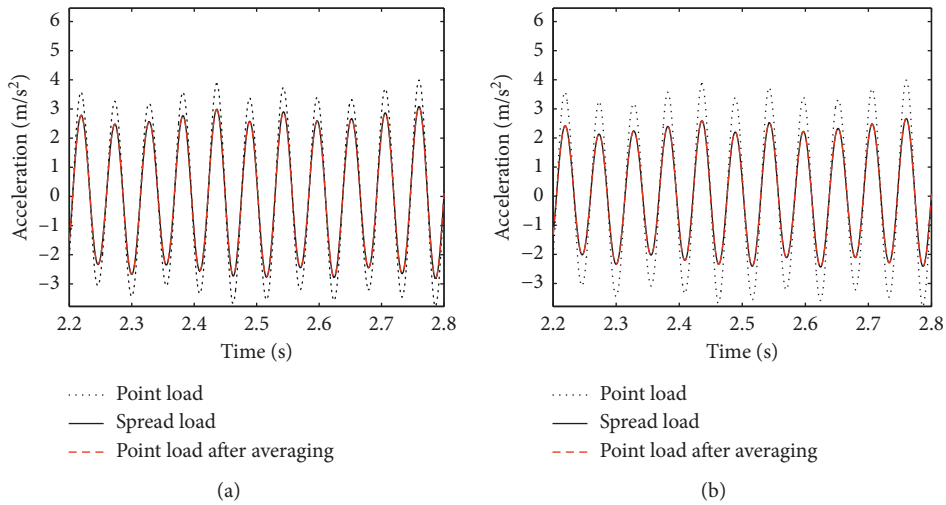

Figure 6: Bridge acceleration time history at resonance speed (ML model). (a) EC block load. (b) Triangular load.

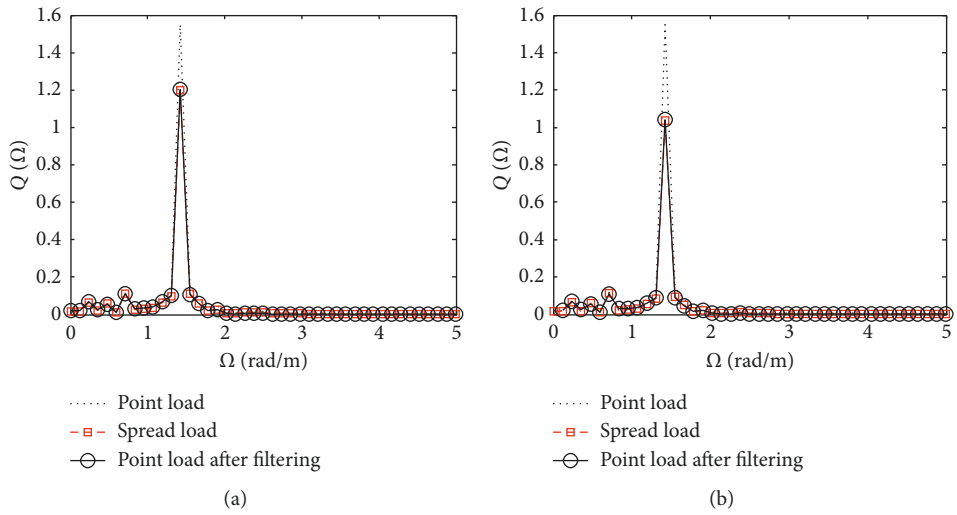

Figure 7: Bridge acceleration spectrum at resonance speed (ML model). (a) EC block load. (b) Triangular load.

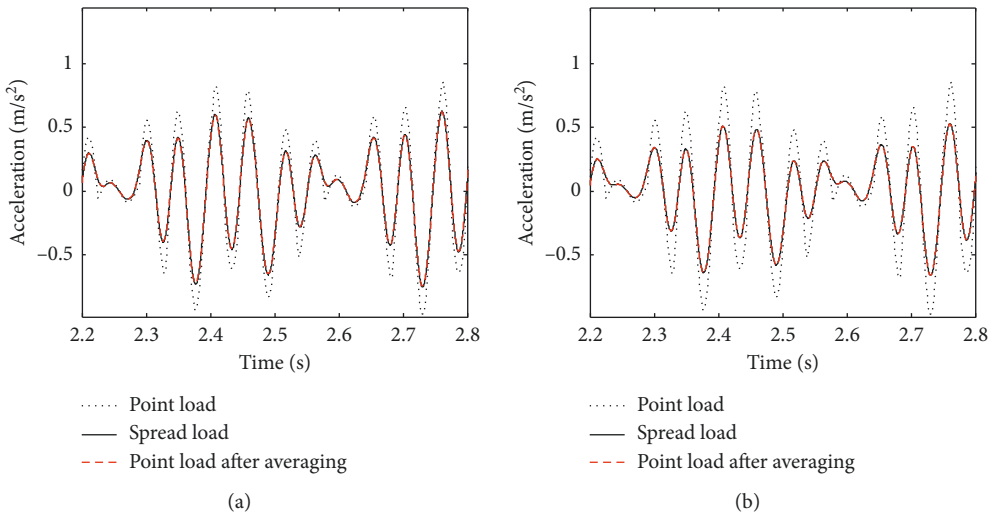

Figure 8: Bridge acceleration time history at nonresonance speed (ML model). (a) EC block load. (b) Triangular load.

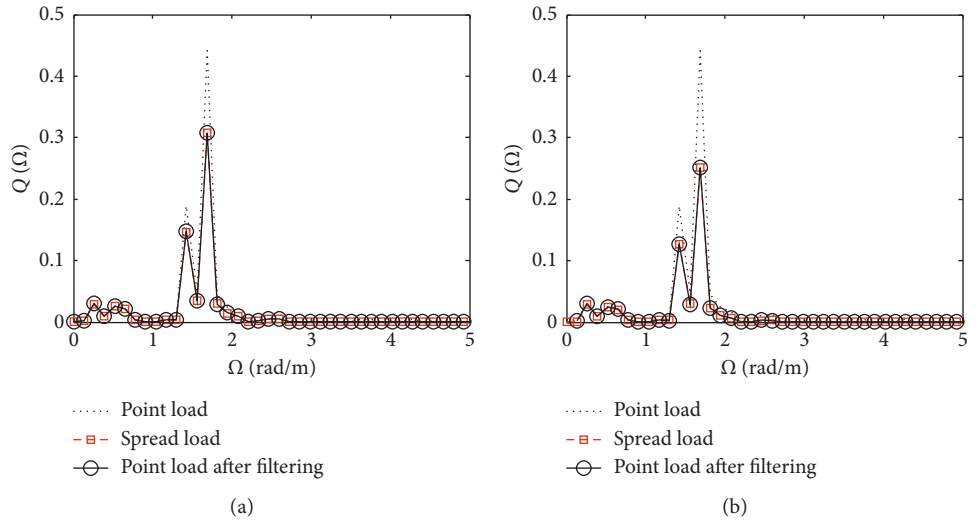

Figure 9: Bridge acceleration spectrum at resonance speed (ML model). (a) EC block load. (b) Triangular load.

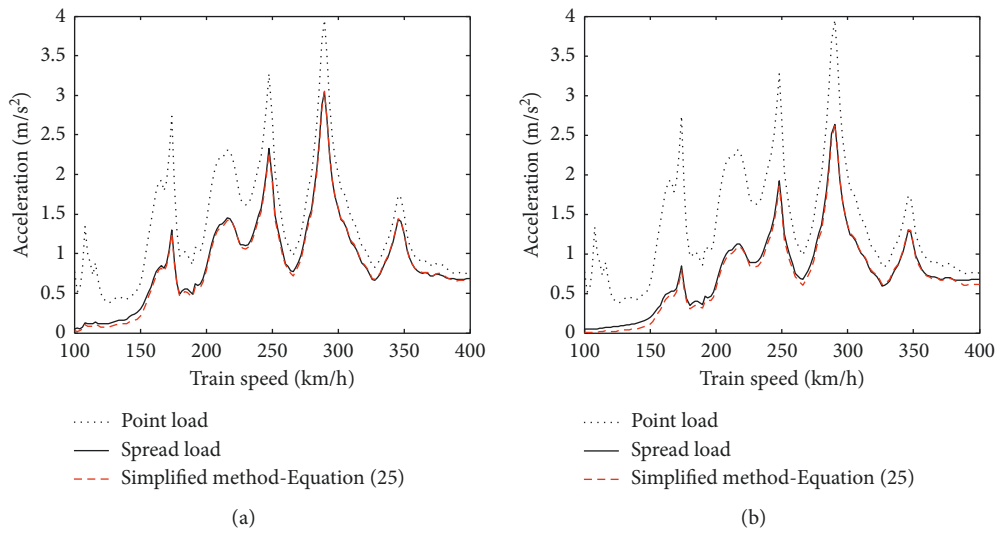

Figure 10: Maximum bridge acceleration (ML model). (a) EC block load. (b) Triangular load.

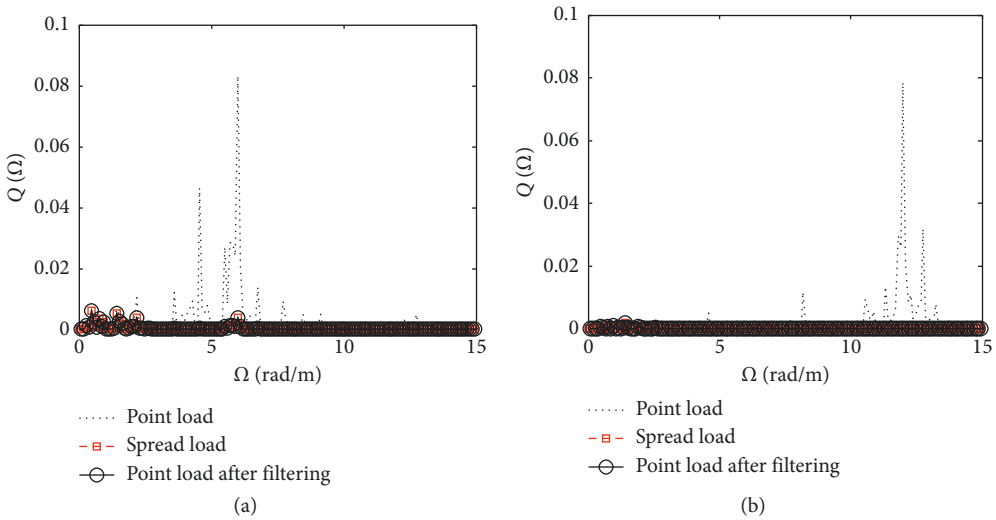

Figure 11: Fourier spectrum of bridge acceleration for the 2nd and the 3rd modes (ML model). (a) The second mode. (b) The third mode.

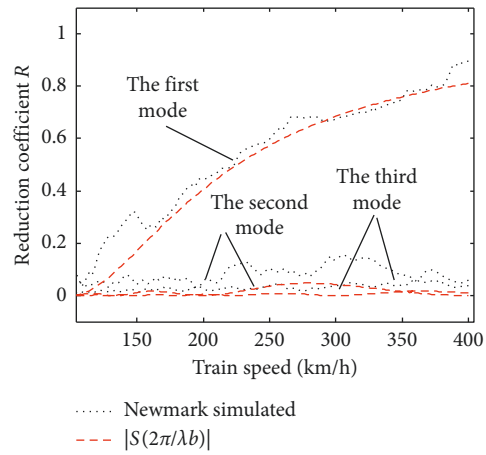

Figure 12: Reduction of bridge acceleration from spread load for the 1st mode to the 3rd mode (ML model).

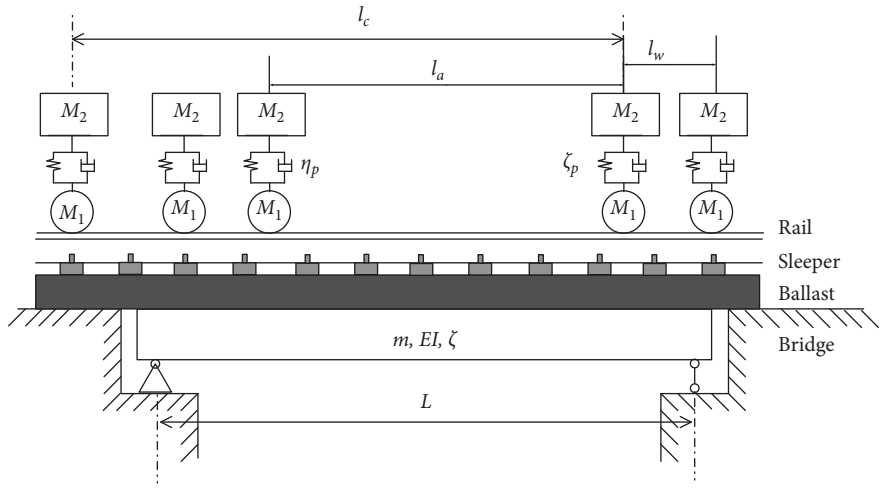

Figure 13: Configuration of the vehicle-bridge dynamic interaction system.

Table 2: Mechanical characteristics of the high-speed train.

Item	Meaning	Unit	Passenger-car	Locomotive
l_c	Length of a vehicle	m	26.1	19.2
l_a	Distance between two trucks in one vehicle	m	$0.68l_c$	12
$2w$	Load distribution width	m	3	3
M_2	Mass of the truck	kg	9937.5	15942
M_1	Mass of the axle	kg	1583	2059
n_p	Natural frequency of the car	Hz	3.85	4.83
ζ_p	Damping ratio of the car	%	11.22	12.90

are the same as those adopted in Section 5. The axle load is assumed to be spread over 3 m as a triangular shape.

The accelerations of the eight bridges due to moving point loads and spread loads obtained by numerical simulation are shown in Figure 15. Figures 15(a) and 15(b) are obtained from the moving load model. Figures 15(c) and 15(d) are those from the vehicle-bridge interaction model. The reduction results for spread load according to (25) are also shown in Figure 15. It can be seen from Figure 15, for the eight bridges considered, that (25) predicts the bridge response due to spread loads very well. The reduction effect of load spreading is more obvious for shorter spans. This is easy to be understood, since the load spreading acts as a low-pass filter, and the short spans have higher natural frequencies.

Figure 16 compares the reduction coefficients from the UIC document [22], (25), and that from numerical simulations. In Figure 16, the reduction coefficient proposed by the UIC document represents a upper bound of the numerical results, while the (25) runs through the results of numerical simulation.

It should be pointed out that the UIC document only gives a graphic reduction coefficient associated with specific load shape and spread lengths of 3 m and 2.5 m. Equation (25) provides a formula that depends explicitly on the wavelength of excitation and the load spread width. Further, the formula can be extended to other load spreading functions.

Figure 17 shows the relative error of the reduction coefficient (25) compared with the reduction obtained through

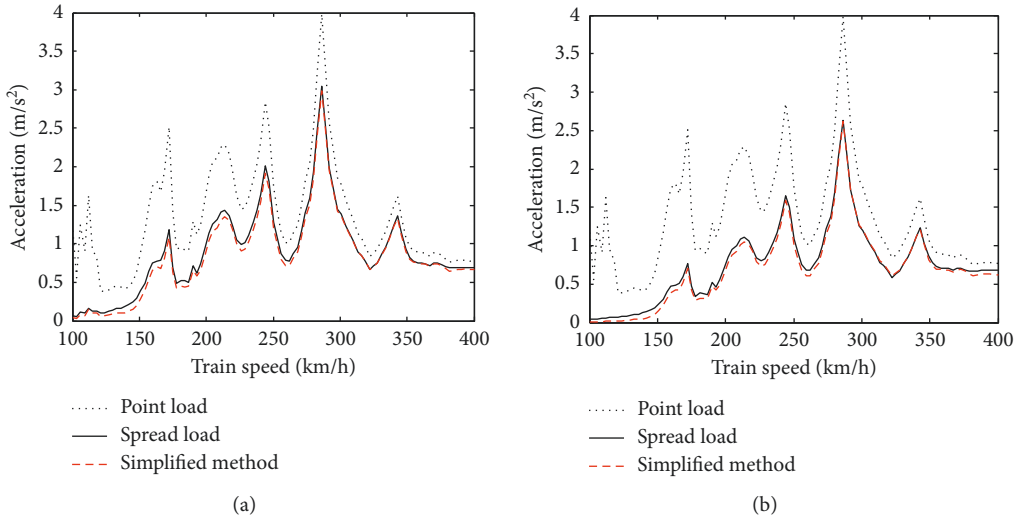

Figure 14: Maximum bridge acceleration (VBI model). (a) EC block load. (b) Triangular load.

Table 3: Mechanical characteristics of the eight simply supported bridges.

Span (m)	Natural frequency (Hz)	Mass per length (kg/m)
6	41.4	6400
8	26.3	10000
10	18.5	9100
12	13.0	12000
14	10.0	13000
16	8.7	13500
18	7.2	14600
20	6.0	16000

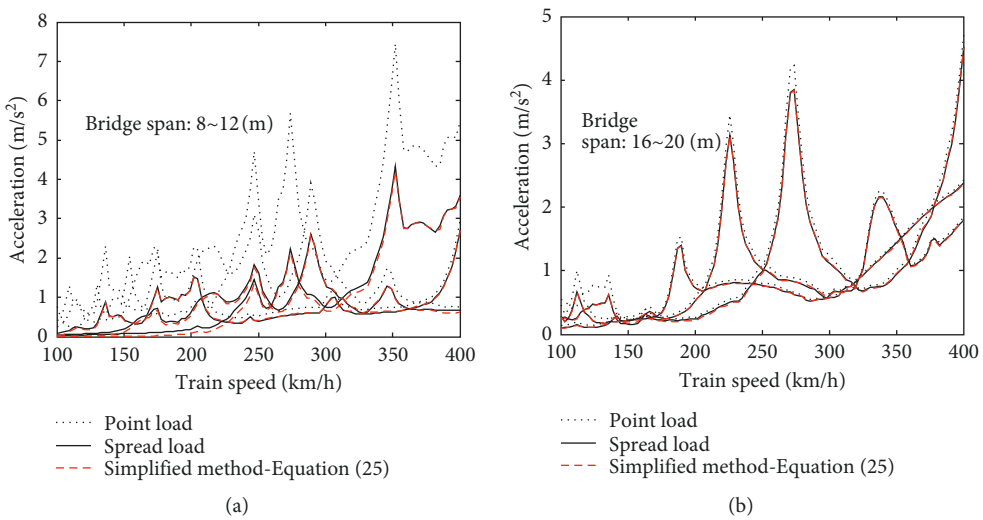

Figure 15: Continued.

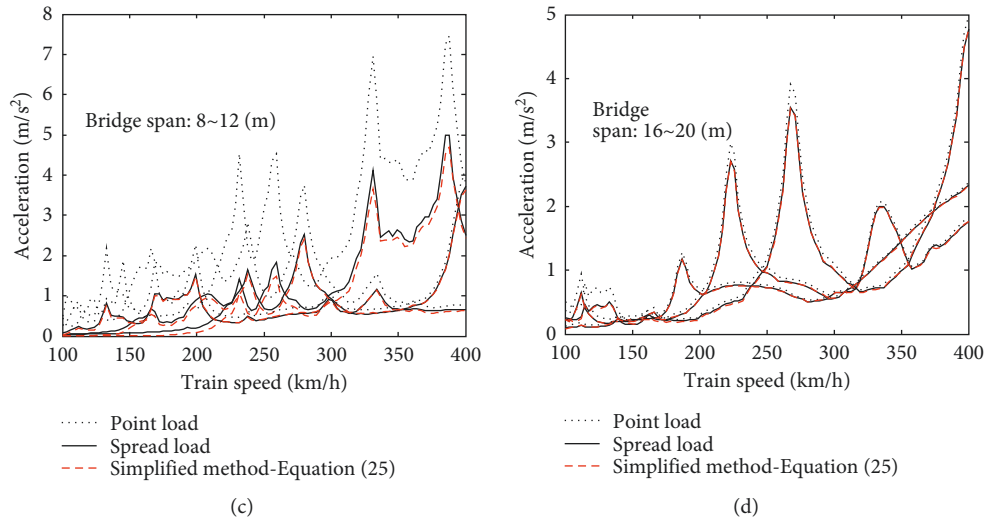

Figure 15: Maximum acceleration of the eight example bridges. (a) Span = 8~12 m (ML model), (b) span = 16~20 m (ML model), (c) span = 8~12 m (VBI model), and (d) span = 16~20 m (VBI model).

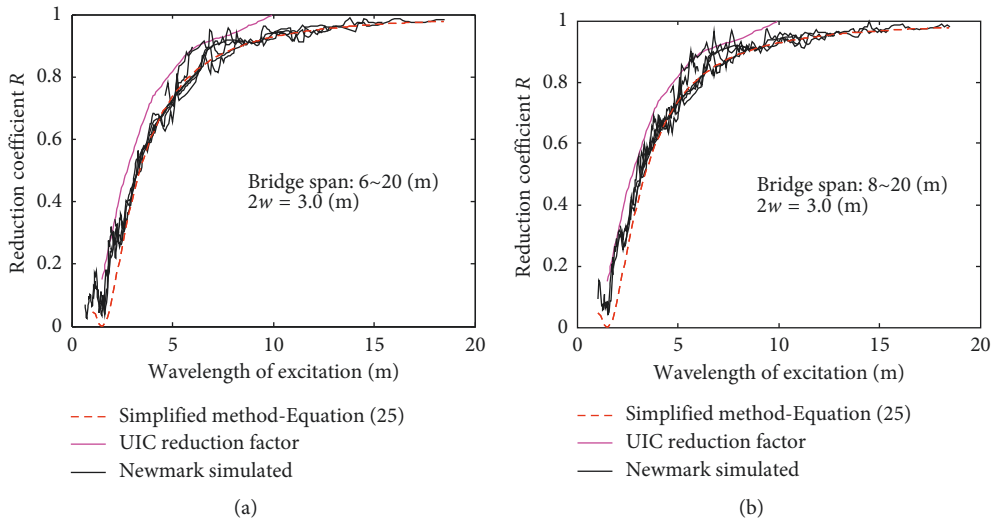

Figure 16: Reduction coefficient from load spreading. (a) ML model. (b) VBI model.

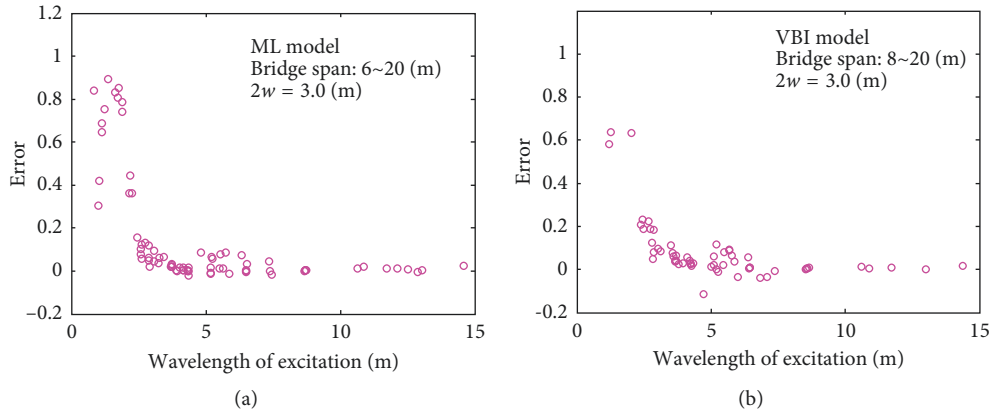

Figure 17: Relative error of the reduction coefficient (25).

numerical simulations. In producing Figure 17, only the resonance peaks which are of practical significance are accounted for. It can be seen that when the wavelength of excitation is larger than 2.7 m, the relative error given by (25) is less than 20%. At the small wavelength side, the bridge vibration is very small (Figure 15) which will not control the bridge design.

7. Conclusion

The vibration of short span railway bridges excited by passing trains was investigated analytically in this study. Moving axle loads from the passing vehicles are modeled as spread loads instead of simplified point loads, which was found to lead to overestimation of short span bridge responses.

In this study, the bridge response predicted using the spread load model was compared to that from using the point load model. In the time domain, the bridge response due to spread loads is proved to be equivalent to a windowed average of the point loads responses, with the spread load shape as the moving window. In the frequency domain, the bridge response due to spread loads can be obtained by passing the point loads result through a low-pass filter. This low-pass filter is the Fourier transform of the load spreading function.

Based on the low-pass filtering process, a simple reduction coefficient was proposed to account for the influence of load spreading effect on bridge vibrations. This coefficient can be calculated as the value of the low-pass filter at the wavelength of excitation, i.e., the ratio of the train speed to the bridge natural frequency. Therefore, this reduction coefficient depends only on the load spreading function and the wavelength of excitation and can be derived in closed-form.

The accuracy of this reduction coefficient in estimating the effect of load spreading on bridge vibrations was validated through numerical simulations. The difference between the reduction of bridge responses given by the proposed formula and that by numerical simulations is less than 20%, provided that the wavelength of excitation is less than 2.7 m. This reduction coefficient is shown to be applicable both for the moving load model and the vehicle-bridge dynamic interaction model.

This study proved the filtering effect of load spreading through the track on bridge vibration. It also provided a simple reduction coefficient to account for this effect without explicitly introducing the track structure model into ML or VBI models.

Data Availability

The data used to support the findings of this study are available from the corresponding author upon request.

Conflicts of Interest

The authors declared no potential conflicts of interest with respect to the research, authorship, and/or publication of this article.

Acknowledgments

The project has received funding from the National Natural Science Foundation of China (grant no. 51678490), Sichuan Province Youth Science and Technology Innovation Team of China (grant no. 2015TD0004), and Science & Technology Department of Sichuan Province (grant no. 2016HH0036).

References

[1] H. Xia, N. Zhang, and G. D. Roeck, "Dynamic analysis of high speed railway bridge under articulated trains," *Computers & Structures*, vol. 81, no. 26-27, pp. 2467–2478, 2003.

[2] Y. B. Yang, J. D. Yau, and Y. S Wu, *Vehicle-Bridge Interaction Dynamics, with Applications to High-Speed Railways*, World Scientific, Singapore, 2004.

[3] Y. L. Xu, N. Zhang, and H. Xia, "Vibration of coupled train and cable-stayed bridge systems in crosswinds," *Engineering Structures*, vol. 26, no. 10, pp. 1389–1406, 2004.

[4] Y. Li, S. Qiang, H. Liao, and Y. L. Xu, "Dynamics of wind–rail vehicle–bridge systems," *Journal of Wind Engineering and Industrial Aerodynamics*, vol. 93, no. 6, pp. 483–507, 2005.

[5] W. M. Zhai, H. Xia, C. B. Cai et al., "High-speed train–track–bridge dynamic interactions, Part I: theoretical model and numerical simulation," *International Journal of Rail Transportation*, vol. 1, no. 1-2, pp. 3–24, 2013.

[6] S. P. Timoshenko, *History of Strength of Materials: With a Brief Account of the History of Theory of Elasticity and Theory of Structures*, McGraw-Hill, New York, NY, USA, 1953.

[7] L. Fryba, *Vibration of Solids and Structures under Moving Loads*, Noordhoff, Groningen, Netherlands, 1972.

[8] Y. B. Yang, J. D. Yau, and L. C. Hsu, "Vibration of simple beams due to trains moving at high speeds," *Engineering Structures*, vol. 19, no. 11, pp. 936–944, 1997.

[9] E. Savin, "Dynamic amplification factor and response spectrum for the evaluation of vibrations of beams under successive moving loads," *Journal of Sound and Vibration*, vol. 248, no. 2, pp. 267–288, 2001.

[10] J. Domínguez, *Dinámica de puentes de ferrocarril para alta-velocidad: Métodos de cálculo y estudio de la resonancia*, Ph.D. thesis, Escuela Técnica Superior de Ingenieros de Caminos, Canales y Puertos, Univ. Politécnica de Madrid, Madrid, Spain, 2001, in Spanish.

[11] H. Xia, N. Zhang, and W. W. Guo, "Analysis of resonance mechanism and conditions of train-bridge system," *Journal of Sound and Vibration*, vol. 297, no. 3–5, pp. 810–822, 2006.

[12] CEN, "Annex E. Limits of validity of load model HSLM and the selection of the critical universal train from HSLM-A," in *Eurocode 1: Actions on Structures—Part 2: Traffic Loads on Bridges*, pp. 141–149, European Committee for Standardization, Brussels, Belgium, 2003.

[13] UIC, "Design requirements for rail-bridges based on interaction phenomena between train, track and bridge," in *Fundamental Hypotheses Relating to Vehicles (Excitation)*, pp. 24-25, International Union of Railways, Paris, France, 2009.

[14] A. Doménech, P. Museros, and M. D. Martínez-Rodrigo, "Influence of the vehicle model on the prediction of the maximum bending response of simply-supported bridges under high-speed railway traffic," *Engineering Structures*, vol. 72, pp. 123–139, 2014.

[15] P. Museros, M. L. Romero, A Poy, and E Alarcón, "Advances in the analysis of short span railway bridges for high-speed

lines," *Computers & Structures*, vol. 80, no. 27–30, pp. 2121–2132, 2002.

[16] T. Arvidsson and R. Karoumi, "Train–bridge interaction–a review and discussion of key model parameters," *International Journal of Rail Transportation*, vol. 2, no. 3, pp. 147–186, 2014.

[17] Y. S. Cheng, F. T. K. Au, and Y. K. Cheung, "Vibration of railway bridges under a moving train by usingbridge-track-vehicle element," *Engineering Structures*, vol. 23, no. 12, pp. 1597–1606, 2001.

[18] B. Biondi, G. Muscolino, and A. Sofi, "A substructure approach for the dynamic analysis of train track-bridge system," *Computers & Structures*, vol. 83, no. 28–30, pp. 2271–2281, 2005.

[19] C. Rigueiro, C. Rebelo, and L. Simões da Silva, "Influence of ballast models in the dynamic response of railway viaducts," *Journal of Sound and Vibration*, vol. 329, no. 15, pp. 3030–3040, 2012.

[20] C. Rebelo, L. Simões da Silva, C. Rigueiro, and M. Pircher, "Dynamic behaviour of twin single-spanballasted railway viaducts–field measurements and modal identification," *Engineering Structures*, vol. 30, no. 9, pp. 2460–2469, 2008.

[21] R. Rehnström and W. Daniel, "*The influence of ballast on the vibrations of railway bridges*," M.S. thesis, Royal Institute of Technology (KTH), Stockholm, Sweden, 2012.

[22] UIC, "Design requirements for rail-bridges based on interaction phenomena between train, track and bridge," in *Appendix B-Criteria to be Satisfied in the Case Where a Dynamic Analysis is Not Required*, pp. 38–41, International Union of Railways, Paris, France, 2009.

[23] C. Johansson, T. Arvidsson, D. Martino et al., *Höghastighetsprojekt Bro–Inventering av Järnvägsbroarför ökad Hastighet Påbefintliga Broar*, Royal Institute of Technology (KTH), Stockholm, Sweden, 2011.

[24] CEN, "Distribution of axle loads by the rails, sleepers and ballast," in *Eurocode 1: Actions on Structures-Part 2: Traffic Loads on Bridges*, CEN, European Committee for Standardization, Brussels, Belgium, 2007.

[25] J. D. Yau, Y. B. Yang, and S. R. Kuo, "Impact response of high speed rail bridges and riding comfort of rail cars," *Engineering Structures*, vol. 21, no. 9, pp. 836–844, 1999.

[26] N. Zhang, H. Xia, and W.W. Guo, "Vehicle–bridge interaction analysis under high-speed trains," *Journal of Sound and Vibration*, vol. 309, no. 3–5, pp. 407–425, 2008.